Extrachromosomal Telomeres Derived from Excessive Strand Displacements

Junyeop Lee[1], Jina Lee[1,2], Eric J. Sohn[1], Angelo Taglialatela[3], Roderick J. O'Sullivan[4], Alberto Ciccia[1,3,5], and Jaewon Min[1,2,5, *]

[1]Institute for Cancer Genetics, Columbia University Vagelos College of Physicians and Surgeons, New York, NY, USA

[2]Department of Pathology and Cell Biology, Columbia University Vagelos College of Physicians and Surgeons, New York, NY, USA

[3]Department of Genetics and Development, Columbia University Vagelos College of Physicians and Surgeons, New York, NY, USA

[4]Department of Pharmacology and Chemical Biology, UPMC Hillman Cancer Center, University of Pittsburgh, Pittsburgh, PA, USA

[5]Herbert Irving Comprehensive Cancer Center, Columbia University Vagelos College of Physicians and Surgeons, New York, NY, USA

*Correspondence to: JM5092@cumc.columbia.edu

Abstract

Alternative Lengthening of Telomeres (ALT) is a telomere maintenance mechanism mediated by break-induced replication (BIR), evident in approximately 15% of human cancers. A characteristic feature of ALT cancers is the presence of C-circles, circular single-stranded telomeric DNAs composed of C-rich sequences. Despite the fact that extrachromosomal C-rich single-stranded DNAs (ssDNAs), unique to ALT cells, are considered potential precursors of C-circles, their generation process remains undefined. Here, we introduce a highly sensitive method to detect single stranded telomeric DNA, called 4SET (Strand-Specific Southern-blot for Single-stranded Extrachromosomal Telomeres) assay. Utilizing 4SET, we are able to capture C-rich single stranded DNAs are near 500 bp in size. Both C-rich ssDNAs and C-circles are abundant in cytoplasmic fraction which supports the idea that C-rich ssDNAs may indeed precede C-circles. We also found that C-rich ssDNAs originate during Okazaki fragment processing in lagging strands. The generation of C-rich ssDNA requires CST-PP (CTC1/STN1/TEN1-PRIMASE-Polymerase alpha)-complex mediated priming of the C-strand synthesis and subsequent excessive strand displacement of C-rich strand through DNA Polymerase delta and BLM helicase. Our work proposes a new model for the generation of C-rich ssDNAs and C-circles that are indicative of the presence of ALT pathway.

Introduction

Telomeres are repetitive sequences consisting of TTAGGG at the ends of chromosomes (1). With each cell division, telomeres undergo progressive shortening due to the end replication problem. Consequently, during tumorigenesis, cancer cells acquire a mechanism to maintain telomere length in order to undergo neoplastic transformation. One such mechanism is the alternative lengthening of telomeres (ALT), which operates independently of telomerase and elongates telomeres through recombination-dependent processes known as break-induced replication (BIR) (2-6). ALT cancers are characterized by ALT-associated specific markers, including ALT-associated PML bodies (APBs) and extrachromosomal telomeric circular DNAs, such as C-circles (C-rich sequences (CCCTAA) containing single stranded circular telomeric DNAs) and T-circles (t-loop sized circle; double stranded circular telomeric DNAs) (7).

T-circles, which can be visualized using electron microscopes or high-resolution STORM microscopes, are generated through processes involving telomere trimming, I-loop (internal- loop) resolution, and looping out during replication processes (8-12). One well-characterized mechanism for T-circle generation is the involvement of TZAP, a negative regulator of telomere length implicated in telomere trimming (13). Notably, T-circles are not only abundant in ALT cancer cells but also present in telomerase-positive cells and germ cells, which possess very long telomeres (14,15). Notably, these T-circles are generated in PML bodies (12).

C-circles are initially found in ALT cancer and ALT-positive immortalized cell lines (16), making them valuable diagnostic markers for ALT cancer (17-19). These circular DNA molecules are present in low abundance and are mostly detectable through the use of

phi29 polymerase (16). Interestingly, recent observations have shown that C-circles are also present in very long telomere-containing fibroblasts, even in cases where ALT is not involved (20). Furthermore, C-circles seem to preferentially exist in the lagging strand (21,22). The generation of C-circles in ALT cancer cells is thought to be related to replication stresses experienced during S phases (23). These replication stresses could potentially activate the ALT pathway and lead to the formation of C-circles. However, the precise process by which C-circles are generated in ALT cancer cells remains unclear, necessitating further research to uncover the underlying mechanisms.

Apart from telomeric circular DNAs, ALT telomeres display various other structures, including T-bands, 5’ overhangs, and single-stranded telomeric DNAs (24,25). T-bands and 5’ overhangs are predominantly observed in the chromatin fraction (25). The presence of 5’ overhangs is likely a consequence of telomere trimming, as they can be detected during T-circle generation processes (15). Notably, a recent study has revealed that T-bands are derived from template switching during BIR-mediated ALT telomere synthesis (26).

Single-stranded telomeric DNAs, on the other hand, are extrachromosomal structures that are enriched in the cytoplasmic fraction obtained by Hirt Lysate (24,25). These single-stranded extrachromosomal telomeric DNAs are believed to serve as potential precursors for C-circles. However, the specific process through which extrachromosomal C-rich single-stranded telomere DNA generation occurs remains unclear and requires further investigation to understand its underlying mechanisms.

In this study, we developed the 4SET (Strand-Specific Southern-blot for Single-stranded Extrachromosomal Telomeres) assay, a simple and efficient method for detecting these

telomeres. Using 4SET, we are able to capture telomeric DNA fragments that contain C-rich single stranded strands of DNA that can be easily measured, near 500 bp in size. Both C-rich ssDNAs and C-circles are abundant in cytoplasmic fraction which supports the idea that C-rich ssDNAs are potential precursors of C-circles. We also found that C-rich ssDNAs are generated during Okazaki fragment processing in lagging strands. The generation of C-rich ssDNA requires CST-PP (CTC1/STN1/TEN1-PRIMASE-Polymerase alpha)-complex mediated priming of the C-strand synthesis and subsequent excessive strand displacement of C-rich strand through DNA Polymerase delta. Our work proposes a new model for the generation of C-rich ssDNAs and C-circles that are indicative of the presence of ALT pathway.

Materials and Methods

Reagents

Mirin (Selleckchem, SML1839; Sigma-aldrich, M9948), PFM01 (Sigma-Aldrich, SML1735), PFM39(Sigma-Aldrich, SML1839), Talazoparib (Selleckchem, S7048), aphidicolin (Sigma-Aldrich, A0781), CD437 (Sigma-Aldrich, C5865), Agarose (Sigma-Aldrich, A9539), SSC buffer (Sigma-Aldrich, S6639), CDP-star (Roche, 11685627001), Blocking reagent (Roche, 11096176001), PBS (Genesee, 25-507B), Glycogen (GlycoBlue Coprecipitant, Invitrogen, AM9515), anti-Beta actin (abcam, ab125096), anti-Histone H3 (Cell signaling, 2650), anti-ATRX (Santa Cruz, sc-15408), anti-hMRE-11 (Calbiochem, PC388), anti-GAPDH (Cell signaling, 97166), TB Green Premix Ex Taq II (Tli RNase H Plus) (Takara, #RR820A), RevertAid First Strand cDNA synthesis kit

(Thermo scientific, K1621), Lipofectamine 3000 (Thermo scientific, L3000001), TransIT (Mirus, MIR2300), Qubit dsDNA HS Assay Kit (Invitrogen, Q32851), Nylon Membranes-positively charged, (Roche, 11417240001), exo$^-$ Klenow fragment (NEB, M0212), T4 DNA polymerase (NEB, M0203), Lambda exonuclease (NEB, M0262), DIG-dUTP (biorbyt, orb533128), NxGen phi29 (Biosearch Technologies, 30221)

Cell culture

U2OS, SaoS2 and HeLa LT cells were maintained in Dulbecco's Modified Eagle Medium (DMEM) supplemented with 10% fetal bovine serum, Penicillin-Streptomycin (Gibco, 15070063). To prevent mycoplasma contaminations, we regularly used Plasmocin Prophylactic (InvivoGen) to maintain the cells according to the manufacturer’s protocol.

siRNA-mediated knockdown

siRNA oligos were purchased from Sigma-Aldrich (10 nmol) and purified by desalting. The dTdT overhangs were added to ensure the stability of siRNA. The siRNAs were transfected into the cells at a final concentration of 20 nM, along with 2 μl of Lipofectamine 3000 (Thermo scientific) according to the manufacturer's protocol.

The following siRNAs were used:

siLuc: UCGAAGUAUUCCGCGUACGUU,

siDNA2#1: CAGUAUCUCCUCUAGCUAGUU (27),

siDNA2#2: AUAGCCAGUAGUAUUCGAUUU (27),

siFEN1#1: UGACAUCAAGAGCUACUUU (28),

siFEN#2 : CCAUUCGCAUGAUGGAGAA (28),

siPRIMPOL: GAGGAAACCGUUGUCCUCAGUG (29),

siFANCM: AAGCUCAUAAAGCUCUCGGAA (30)

Lentiviral shRNA-mediated knockdown

Lentiviruses were generated by transfecting shRNA vectors targeting human POLD3 (31), STN1 (32), ATRX(33), or the control vector along with pMD2.G and psPAX into 293T cells. Transfection was carried out using TransIT (Mirus) following the manufacturer's protocol. After 24 hours, the medium was replaced with fresh medium, and cells were incubated for an additional 24 hours. Supernatants containing the lentiviruses were collected and passed through a 0.45 μm syringe filter. The collected supernatants were then concentrated using 4x virus concentrator solution. This solution consisted of phosphate-buffered saline (PBS) at pH 7.2 containing 1.2 M sodium chloride and 40% (v/w) PEG-8000. The concentrated virus pellets were used to infect target cells, and 0.5 μg/ml polybrene was added to enhance viral transduction. Cells were selected under either 5 μg/ml Blasticidin-S (Invivogen) for two weeks or 5 μg/ml Puromycin (Invivogen) for 5 days to establish stable cell lines expressing the desired shRNA. Proper biosafety procedures were followed when working with lentiviruses.

Plasmid

cDNA encoding PRIMPOL was synthesized from Integrated DNA Technologies (IDT) and cloned into pCS2(+) NLS-mCherry vector. PRIMPOL S255D mutant was generated using Q5 site-directed mutagenesis kit (NEB). The pCS2 NLS-mCherry-PRIMPOL WT or S255 vectors were used for transfection in U2OS PRIMPOL KO cells using TransIT (Mirus)

according to the manufacturer's protocol. cDNA expression and transfection efficiency were assessed by mCherry signal.

Strand-Specific Southern for Single-stranded Extrachromosomal Telomeres (4SET)

- **DNA preparation procedure**

Cells were harvested using Trypsin-EDTA and then divided into separate tubes for fractionation. The cells were pelleted via centrifugation (500 g, 5 min) and washed with PBS. For the whole DNA fraction, cells were lysed by adding lysis buffer (0.1 M Tris pH 8.0, 0.1 M EDTA, 1% SDS). To obtain the nucleus and cytoplasm fractions, cells were treated with Membrane lysis buffer (PBS, 5 mM EDTA, 0.1% Triton X-100) and subjected to pipetting over ten times. The cell lysate was subsequently centrifuged at 1500 g for 5 min to separate the nucleus pellet from the cytoplasmic supernatant. The nucleus pellet was then lysed using lysis buffer. After obtaining the whole, nuclear, and cytoplasmic fractions, NaCl was added to each fraction (final concentration 1.6 M NaCl). The fractions were then centrifuged at 4°C, 15,000 g for 20 minutes to remove cell debris and obtain the DNA-containing supernatant. To precipitate the DNA, Glycogen (GlycoBlue Coprecipitant) was added to the supernatant, followed by the addition of 75% of the supernatant volume of isopropanol. The mixture was subjected to additional centrifugation at 4°C, 15,000 g for 20 minutes to obtain the DNA pellet. Subsequently, the DNA pellet was washed twice with 70% ethanol by centrifuging at 15,000 g for 5 minutes each time. Finally, the DNA pellet was dissolved in DW (distilled water) and incubated overnight at 4 °C to ensure complete dissolution. The DNA concentration was measured using Qubit (Qubit dsDNA HS Assay Kit, Invitrogen) or a nanodrop spectrophotometer.

- **Southern blot procedure**

For electrophoresis, 210 ng of whole DNA, measured using Qubit, was loaded into 0.6% Agarose gel and run at 40 V (2.9V/cm) in TAE (Tris-acetate EDTA) buffer. Subsequently, the agarose gel underwent sequential incubations in the following solutions: Depurination solution (0.2 M HCl) for 5 minutes, Denaturation solution (0.5 M NaOH, 1.5 M NaCl) for 5 minutes, and Neutralization Buffer (0.5 M Tris pH 8.0, 1.5 M NaCl) for 20 minutes. The DNA was then transferred onto a Nylon membrane (Nylon Membranes, positively charged, Roche) using a Vacuum Blotting System (VacuGene XL) at 30 mbar for 1 hour in 4xSSC (Saline Sodium Citrate) buffer. Following this, the membrane was incubated with 1 nM DIG (Digoxigenin)-labeled Telomere probes in Hybridization solution (DIG Easy Hyb, Roche) at 42°C. Afterward, the membrane underwent two washes with Wash buffer 1 (2xSSC, 0.1% SDS) and two washes with Wash buffer 2 (0.5xSSC, 0.1% SDS) for 10 minutes each. The membrane was then blocked with Blocking solution (1% Blocking reagent in Maleic acid buffer pH 7.4) for 30 minutes, followed by incubation with 0.2% Anti-Digoxigenin-AP Fab fragments (Roche) in Blocking solution for 1 hour. Subsequently, the membrane underwent two washes with Wash buffer 3 (Maleic acid, 0.3% tween-20) for 15 minutes each. Finally, the membrane was incubated with 1% CDP-star (Roche) in AP buffer (50 mM Tris pH 9.5, 100 mM NaCl) for detection, which was performed using the Odyssey Imaging System (LI-COR 2800).

- **Strand specific probe generation procedure**

To produce strand-specific probes, minor modifications were made to the previous protocol (34). Annealed templates (TC, TG, and UP* in the list below) were generated at a concentration of 40 μM in NEBuffer#2.1 (NEB) buffer. The templates were then

incubated with 50 units of exo-Klenow enzyme (NEB) and 1 mM dNTP with 0.35 mM DIG-dUTP (biorbyt) at 25°C overnight, followed by heat inactivation at 75°C for 20 minutes. Subsequently, we performed a 10-unit T4 DNA polymerase reaction to improve specificity. The double-stranded oligos were purified using NucleoSpin Gel and PCR clean-up (MN) using NTI buffer following the manufacturer's instructions. Next, a 20-unit lambda exonuclease reaction was carried out to obtain single-stranded oligos for 1 hour at 37°C. Finally, the single-stranded telomere probes were purified using NucleoSpin Gel and PCR clean-up (MN) using NTC buffer.

Following oligos were used:

Telomere C-rich probe template (TC):

5'[Phos]GGGTTAGGGTTAGGGTTAGGGTTAGGGTTAGGGTTAGGGTTAGATAGTTGAGAGTC-3'

Telomere G-rich probe template (TG):

5'[Phos]CCCTAACCCTAACCCTAACCCTAACCCTAACCCTAACCCTAGATAGTTGAGAGTC-3'

Universal priming oligo (UP*): 5'-[Phos]GACTCTCAAC*T*A*T*C*T*A-3'

(*) indicates phosphorothioate bond.

C-circle assay

Genomic DNAs were subjected to incubation with 10 units of phi29 polymerase (NxGen phi29), 0.2 mM dNTP mix, and 1X phi29 buffer at 30°C for 12 hours, followed by a 20-minute incubation at 65°C. Subsequently, the samples were loaded onto a Nylon

membrane using a slot-blot technique. The subsequent steps of hybridization and detection followed the same procedure as described in the 4SET method.

Western Blot

The cell pellet, nucleus pellet, and cytoplasm supernatant were treated with Laemmli loading buffer (2% SDS, 5% beta-mercaptoethanol, 10% Glycerol, 0.002% Bromophenol Blue, 62.5 mM Tris-base) and subjected to 10 seconds of ultrasonication. The prepared samples were then separated on a Bis-Tris 4~12% polyacrylamide gel and transferred to a PVDF membrane using the iBlot 2 Dry Blotting System. After blocking with 5% skim milk in PBS-T (PBS-0.1% Tween-20) for 1 hour at room temperature, the membrane was incubated with the primary antibody overnight at 4°C. Following PBS-T wash, the membrane was incubated with the secondary antibody for 1 hour at room temperature. After an additional PBS-T wash, the ECL solution was applied, and detection was performed using the Odyssey Imaging System (LI-COR 2800).

Antibodies

The following antibodies were used for Western Blot: anti-Beta actin (abcam, ab125096), anti-Histone H3 (Cell signaling, 2650), anti-ATRX (Santa Cruz, sc-15408), anti-hMRE-11 (Calbiochem, PC388), anti-GAPDH (Cell signaling, 97166)

RNA extraction and quantification

For RNA quantification, total RNA was extracted by using Direct-zol RNA Miniprep kits (ZYMO) according to the manufacturer's protocol. cDNAs were synthesized using RevertAid First Strand cDNA synthesis kit (Thermo scientific) and qPCRs were performed

using TB Green Premix Ex Taq II (Tli RNase H Plus) (Takara) according to the manufacturer's protocol.

The following DNA probes were used for qPCR:

GAPDH F: TGAGAACGGGAAGCTTGTCA,

GAPDH R: AGCATCGCCCCACTTGATT,

STN1 F: TGCACAGAAAGATCCACCGG,

STN1 R: AGGCCAAGATGTGCAGGAA,

DNA2 F: ACTGTGAAAAGCGCCTGGT,

DNA2 R: AGATGTGCAGTCTCCCTCCA,

FEN1 F: TTCTTCAAGGTGACCGGCTC,

FEN1 R: TTAAACTTCCCTGCTGCCCC

Statistical Analyses

Statistical analyses for the experiments were conducted using GraphPad Prism 8. The graph displays all individual values. Detailed information regarding the tests and corresponding p-values is provided in the figures and their respective legends.

Result

4SET assay, a simple and efficient method for detecting single-stranded extrachromosomal telomeric DNA.

To investigate the abundance of single-stranded telomeric DNA in ALT cancer, we have made modifications to existing Southern protocols that we named 4SET (Strand-Specific Southern-blot for Single-stranded Extrachromosomal Telomeres) (Fig. 1A). These modifications were aimed at enhancing sensitivity and optimizing the protocol specifically for the detection of single-stranded DNA. First, we optimized the genomic DNA extraction procedure for single-stranded DNA fragments. It has been observed that the isopropanol/ethanol precipitation procedure can result in unreliable nucleotides recovery efficiency, particularly for small nucleic acids when the concentration of nucleic acid is low (35). During isopropanol/ethanol DNA precipitation, the presence of bulk DNA/RNA can act as a carrier which facilitates the precipitation of small-sized nucleic acids. To overcome this issue, we introduced excessive amounts of glycogen as a carrier during the isopropanol precipitation step. Additionally, we incubated the mixture at -20 degrees Celsius for a minimum of 3 hours to maximize the precipitation of single-stranded DNA fragments. Secondly, we ran the genomic DNA on a low-percentage agarose gel and conducted the transfer onto a positively charged nylon membrane instead of using gel dry. This approach was chosen primarily to avoid the loss of small DNA fragments that can occur during the vacuum-based gel drying process. When the gel is dried using a vacuum, there is a risk of small DNA fragments being lost as the moisture is removed from below to dry the gel through the pressure. Lastly, we used highly sensitive strand specific C-rich and G-rich telomere probe to determine strand specificity (34).

Furthermore, we carefully considered the temperature at which we dissolve the precipitated DNA pellet, because single-stranded DNA fragments are not stable at high temperatures such as 55 degrees Celsius. As previously reported, C-circles are also sensitive to temperature and freeze-thaw cycle (16). DNA dissolution temperature also affects C-circle assay due to its stability. We thus used low temperatures for DNA dissolution and avoided freeze-thaw cycle.

Single-stranded telomeres are observed in Hirt lysate, a method used for isolating extrachromosomal DNA (24,25). Consequently, we conducted cell fractionation to investigate the presence of C-rich ssDNAs in the cytoplasm. By employing 0.1% Triton X-100, we separated the cells into a nuclear fraction (pellet) and a cytoplasmic fraction (supernatant) (Fig. 1B). We validated our cell fractionation by Western blot, confirming that histone H3 proteins are present in nuclear and whole fractions, GAPDH proteins are found in cytoplasmic and whole fractions, and beta-actin proteins are enriched in cytoplasmic fractions (Fig. 1C).

We performed 4SET assay after cell fractionation in U2OS and SaoS2 cells, which are commonly used ALT-positive cancer cell lines derived from osteosarcoma patients (Fig. 1D, S1A). Consistent with previous reports (24), SaoS2 cells exhibited bands around 500 bp in size which are C-rich ssDNA (Fig. 1D; G-rich probe). Notably, the cytoplasmic fraction exhibited a substantial abundance of C-rich ssDNAs, while no signal was detected in the nuclear fraction, indicating that C-rich ssDNA predominantly resides in the cytoplasm (Fig. 1D; cytoplasmic DNA). Furthermore, our 4SET method enabled us to detect these small single stranded C-rich telomeres in U2OS cells as well, which were not detected previously (Fig. 1D; U2OS cytoplasmic DNA).

Next, we measured the C-circles by using phi29 polymerase mediated rolling circle amplification after cell fractionation (Fig. 1E). C-circles were also detected more in the cytoplasm, which is consistent with original findings on C-circles (16) (Fig. 1F, S1B).

MRE11 nuclease activity suppresses the generation of C-rich ssDNA.

We investigated which nucleases are responsible for the generation of C-rich ssDNAs and C-circles. We first tested the impact of MRE11 nuclease activity inhibition in the generation of C-circles (Fig. 2A). We used Mirin, a small molecule inhibitor of MRE11 which inhibits MRE11 nuclease activity (36). Surprisingly, C-circles were increased in Mirin-treated condition in both U2OS and SaoS2 cells (Fig. 2B-C). Next, we performed a 4SET assay in Mirin-treated condition (Fig. 2D, S2A). Mirin treatment led to increases in C-rich ssDNAs which are mostly in cytoplasm fractions, still C-rich ssDNAs were not detected in nucleus fraction (Fig. 2D; G-rich probe).

We checked whether the impact of MRE11 inhibition in non-ALT cells to check whether Mirin-induced C-rich ssDNAs generation is ALT-specific phenotype. HeLa LT cells, telomerase-positive cells harboring long telomeres, were used (37). Mirin treatment in HeLa LT cells didn't lead to generation of C-rich ssDNAs (Fig. S2B), indicating that C-rich ssDNAs are ALT cancer specific phenotype as previously documented (24).

Lastly, we tested other MRE11 nuclease inhibitors, PFM01 and PFM39 which are derived from Mirin structure-based chemical screening (38). Both PFM01 and PFM39 treatments also increased C-rich ssDNAs (Fig. S2C), confirming that the impact of Mirin treatment is due to the inhibition of nuclease activity of MRE11.

C-rich ssDNAs are derived from lagging strand during the Okazaki fragment processing.

It showed that C-circles are produced during telomere replication and are predominantly present in the lagging strand compared to the leading strand (21,22). Telomeres expose their G-rich ssDNAs during Okazaki fragment formation at the lagging strands (39). These G-rich ssDNAs can form higher order structures such as G-quadruplexes, which not only contribute to telomere fragility but also serve as substrates for nucleases, such as MRE11 and DNA2 (39-43).

We observed an increase in C-rich ssDNAs in conditions where MRE11 was inhibited (Fig. 3A), possibly preventing the processing of higher order structures in the lagging strands. Based on this, we hypothesized that C-rich ssDNAs are derived from lagging strand processing. To further investigate this idea, we decided to deplete DNA2, which is also involved in lagging strand processing at telomeres (43). We employed siRNA targeting DNA2 to deplete its levels in U2OS cells (Fig. S3A).

We initially measured C-circle levels in the DNA2 depletion condition (Fig. 3A) and found that, consistent with previous reports, DNA2 depletion resulted in an increase in C-circle levels (Fig. 3B; siDNA2) (37). Interestingly, the combination of DNA2 depletion and Mirin treatment led to even higher C-circle levels, indicating a synergistic effect of inhibiting MRE11 and DNA2 depletion.

This led us to measure the C-rich ssDNAs in DNA2 depleted condition. We thus conducted a 4SET assay in the DNA2 depletion condition (Fig. 3C, S3B). DNA2 depletion alone caused an increase in C-rich ssDNA (Fig. 3C; siDNA2). Moreover, when Mirin was

treated with DNA2 depletion, it further enhanced the accumulation of C-rich ssDNA (Fig. 3C; siDNA2 with Mirin).

As DNA2 has a role in removing the flap structures during Okazaki fragment processing, we tested if other flap nuclease, FEN1 might be involved in C-rich ssDNA generation (44). We depleted FEN1 using siRNA (Fig. S3C). Interestingly, FEN1 depletion led to a moderate decrease in C-circle levels (Fig. 3A, B; siFEN1). In the presence of Mirin treatment, FEN1 depletion led to partial decrease in C-circle levels (Fig. 3A, B; siFEN1 with Mirin). Consistently, FEN1 depletion also led to a partial decrease in C-rich ssDNA generation (Fig. 3D, S3D) with or without Mirin treatment, which is completely opposite to DNA2 depletion result.

DNA2 exhibits a preference for cleaving long-flap structures from the 5' end of the flap, whereas FEN1 is capable of cleaving the middle of the flap, as they are recruited by PCNA (Fig. S3E) (44). We hypothesize that FEN1 nuclease plays a role in generating C-rich ssDNAs by cutting the middle of 5' flap structures when long-flap structures are not adequately processed by DNA2. To test this idea, we conducted a double-depletion experiment, simultaneously targeting FEN1 and DNA2, to determine if double depletion of FEN1 and DNA2 can impede the accumulation of C-rich ssDNAs in the DNA2 depleted condition (Fig. 3E, S3F). Double depletion of FEN1 and DNA2 exhibited decreased the C-rich ssDNAs compared to single DNA2 depletion in both U2OS and SaoS2 cells, indicating that FEN1 is partially contribute to the generation of C-rich ssDNAs, possibly cleaving the flap structures in the lagging strands.

Next, we explored whether the exposed ssDNAs in lagging strand telomeres themselves could contribute to an increase in C-rich ssDNAs. To test this idea, we utilized a PARP

inhibitor, which is known to impact ssDNA generation in lagging strands by perturbing Okazaki fragment maturation (45,46). We applied a modest dosage of Talazoparib, a PARP inhibitor, to induce ssDNA gaps in the lagging strands (47). Remarkably, treatment with the PARP inhibitor resulted in an increase in C-rich ssDNAs, similar to what was observed with Mirin treatment (Fig. S3G), supporting the idea that C-rich ssDNAs are generated during lagging strand processing through ssDNA exposure and gap formation.

In exploring another possibility for the origin of C-rich ssDNAs, we investigated whether they might be generated from the other strand, specifically ssDNA or gaps from the leading strands. To explore this, we focused on PRIMPOL, a Primase-polymerase known for its role in repriming and gap formations in leading strands (29,48,49). Notably, depletion of PRIMPOL did not show any changes in the levels of C-rich ssDNAs (Fig. S3H). Furthermore, we analyzed PRIMPOL knockout cells, which have a defect in gap formation on leading strands in response to DNA replication challenges (50). When we introduced either PRIMPOL wild-type (WT) or the phosphomimic and constitutively active mutant S255D into PRIMPOL knockout cells (51), we observed no changes in C-rich ssDNAs (Fig. S3I). These results also support the idea that C-rich ssDNAs are primarily derived from gap formation on the lagging strands rather than from the leading strands.

ATRX suppresses the generation of C-rich ssDNAs.

Mutations in the ATRX gene have been identified in many ALT cancers, and a significant number of ALT positive cells exhibit loss of ATRX expression (33,52). Recent studies showed that reintroducing the ATRX gene expression using a doxycycline-inducible promoter, in U2OS cells, which lack ATRX due to homozygous deletion, effectively reversed the ALT phenotypes, such as C-circles, APBs, and accumulations of DNA/RNA

hybrids (R-loops) at telomeres (53,54). We used these U2OS^{ATRX} cells to test whether ATRX re-expression in U2OS^{ATRX} cells can affect the generation of C-rich ssDNAs. After 7 days of doxycycline treatment, U2OS^{ATRX} cells express ectopic ATRX (Fig. 4A).

First, we measured C-circle levels in the doxycycline-induced ATRX expression condition (Fig. 4B). As expected, ATRX expression led to a decrease in C-circle levels. Interestingly, ATRX expression also mitigated the increase in C-circles caused by Mirin treatment (Fig. 4B, C; Dox with Mirin), suggesting that the increase in C-circles induced by Mirin treatment is dependent on the absence of ATRX in U2OS cells. Subsequently, we assessed C-rich ssDNAs under the condition of ATRX expression. ATRX expression in U2OS cells decreased the quantity of C-rich ssDNAs, and it alleviated the increase of C-rich ssDNAs induced by Mirin treatment (Fig. 4D, S4A). Additionally, we investigated the impact of ATRX expression in U2OS cells on the elevation of C-circle and C-rich ssDNA levels in DNA2 depleted condition. DNA2 depletion also led to an increase in C-circles in U2OS^{ATRX} cells (Fig. 4E, F; Dox with siDNA2). Doxycycline-induced ATRX expression also mitigated the increase in C-circles by DNA2 depletion. Then we measured the C-rich ssDNAs in ATRX expressing U2OS cells after DNA2 depletion (Fig. 4G, S4B). ATRX expression in U2OS cells diminished the increase of C-rich ssDNAs induced by DNA2 depletion. These results indicate that loss of ATRX is a crucial factor in the generation of C-rich ssDNAs in U2OS cells.

Considering that ATRX is involved in resolving G-quadruplexes (G4) at telomeres and its depletion can lead to the accumulation of R-loop structures at telomeres associated with G4 (53,55), we predicted that DNA/RNA hybrid formation in the leading strand could produce C-rich ssDNAs by causing gaps in the unhybridized strand in the lagging strand.

We found that FANCM depletion, which induces R-loop accumulation at ALT telomeres (30,56), led to an increase in C-rich ssDNAs (Fig. S4C), which is consistent with the previous observation (57). To further validate this idea, we analyzed RAD51AP1 KO cells (58), which are known to exhibit reduced G-quadruplex-associated R-loop formations at ALT telomeres (59-61). RAD51AP1 KO cells displayed lower levels of C-rich ssDNAs compared to Control cells (Fig. S4D). Collectively, these results indicate that loss of ATRX is a crucial factor in the generation of C-rich ssDNAs, likely facilitated by the accumulation of R-loops at telomeres.

Next, to investigate whether the loss of ATRX alone is adequate to induce C-rich ssDNA generation, we introduced shRNA targeting the ATRX gene into HeLa LT cells. Consistent with previous studies demonstrating that the loss of the ATRX gene alone is not sufficient to induce the ALT phenotype (33,62-64), we did not observe the generation of C-rich ssDNAs in HeLa LT cells after ATRX depletion, even when subjected to Mirin or PARPi treatment in our 24-hour treatment experiment (Fig. S4E). These results indicate that ATRX may not be the sole determinant in the regulation of C-rich ssDNA formation in HeLa LT cells under the specific short-term experimental conditions we employed.

CST complex-mediated priming and subsequent strand displacements by DNA polymerase delta generates C-rich ssDNAs.

CST (CTC1/STN1/TEN1)-PP (Primase/DNA polymerase alpha) complex plays a crucial role in the C-strand fill-in processes at telomeres (65). It recognizes exposed G-rich strands, including higher-order structures like as G-quadruplex, on the parental lagging strand during telomere replication and initiates the filling in of the complementary C-strand, generating additional Okazaki fragments that serve to remove the gaps in the lagging

strand and ensure the telomere replication (32,66-69). Because the exposed ssDNAs in lagging strand telomeres are priming sites for CST complex, we hypothesized that C-rich ssDNAs could be generated by additional Okazaki fragments formation by CST complex mediated priming (Fig. 5A). We depleted STN1, a component of CST complex, using shRNA targeting STN1 (32) (Fig. S5A). Consistent with the previous report, depletion of STN1 led to a reduction of C-circles in Mirin-treated U2OS cells (Fig. 5B, C). We performed a 4SET assay to measure the levels of C-rich ssDNAs in conditions where STN1 was depleted. Surprisingly, the depletion of STN1 led to a striking reduction in C-rich ssDNAs in both U2OS and SaOS2 cells (Fig. 5D, S5B). Furthermore, STN1 depletion also resulted in the dramatic abolishment of C-rich ssDNAs in response to Mirin treatment. These findings suggest that STN1 plays a crucial role in the generation of C-rich ssDNAs and highlights its involvement in the response to Mirin treatment in these cells.

Primed Okazaki fragments, created by DNA polymerase alpha, are subsequently extended by DNA polymerase delta (44). This sequential process ensures the continuous synthesis of the lagging strand during DNA replication and creates a flap structure as polymerase delta displaces the downstream DNA strand. Particularly in ALT cells, the excessive strand displacement activity of polymerase delta, working with BLM helicase and other associated factors, plays a crucial role in ALT telomere elongation through BIR (5,70-72). We hypothesized that the primed C-strand Okazaki fragments, initiated by the CST-PP complex, undergo prolonged extension by DNA polymerase delta and BLM helicase, creating a flap structure. This unique excessive strand displacement activity in ALT cells allows for the complete displacement of downstream DNA, resulting in the accumulation of C-rich ssDNA (Fig. 5A).

To test this idea, we depleted POLD3, a component of DNA polymerase delta, using shRNA targeting POLD3 (31,73). Depletion of POLD3 led to a decrease in C-circles in Mirin treated U2OS cells. We conducted a 4SET assay to measure the C-rich ssDNAs in POLD3-depleted cells. Strikingly, POLD3-depletion reduced the C-rich ssDNAs in U2OS cells (Fig. 5E, S5C). Moreover, POLD3-depletion also abolished the C-rich ssDNA in response to Mirin treatment.

To further validate the involvement of DNA polymerase alpha and delta in the generation of C-rich ssDNAs, we conducted 4SET assay after treating low dosages of Aphidicolin (a DNA polymerase alpha/delta inhibitor) and CD437 (a DNA polymerase alpha inhibitor) to partially inhibit their actions. The results were consistent with our hypothesis, as both Aphidicolin and CD437 treatments led to decreases in C-rich ssDNAs (Fig. S5D), confirming that C-rich ssDNAs are indeed derived from lagging strand processes mediated by DNA polymerase alpha and delta. The inhibition of these DNA polymerases resulted in reduced C-rich ssDNA formation, supporting their role in this process during telomere replication.

Consistent with our hypothesis, we observed that BLM knockout cells showed reduced levels of C-rich ssDNAs (Fig. S5E). Furthermore, when we depleted BLM using siRNA specifically targeting BLM, we also observed a decrease in C-rich ssDNAs (Fig. S5F). These results support that BLM helicase is involved in the generation of C-rich ssDNAs in the context of ALT telomere replication through BIR. The reduced levels of C-rich ssDNAs upon BLM depletion suggest that BLM's excessive strand displacement activity likely plays a crucial role in this process.

Furthermore, STN1- and POLD3-depletion also mitigated the increase of C-rich ssDNAs induced by DNA2 depletion (Fig. 5F, S5G), supporting the idea that C-strand synthesis priming followed by excessive strand displacement is required for the generation of C-rich ssDNAs in ALT cells.

Discussion

4SET, a sensitive method to detect extrachromosomal single stranded DNAs.

We demonstrate a highly sensitive and accessible method to detect extrachromosomal telomeric ssDNAs called 4SET (Strand-Specific Southern-blot for Single-stranded Extrachromosomal Telomeres) assay. This technique can be performed within two days by molecular biologists at an intermediate level of expertise, without the need for specialized or expensive laboratory equipment, allowing us to investigate single-stranded extrachromosomal telomeres in a time-efficient and cost-effective manner. Additionally, this assay offers a strand-specific approach, allowing for the discrimination of specific telomere strands during analysis. For example, by employing the 4SET assay, here we proposed the model of underlying mechanisms of generation of single-stranded extrachromosomal telomeres which are derived from strand displacement of lagging strands. Furthermore, the simplicity and efficiency of the 4SET assay make it suitable for implementation in various research settings, such as assessing other repeat sequences of interest.

Generation of C-rich single stranded DNAs are suppressed by MRE11, DNA2 nucleases.

In our study, we explored the roles of MRE11 and DNA2 nucleases in the generation of C-rich single-stranded DNAs. MRE11, along with RAD50 and NBS1 forms MRN complex, is involved in DNA repair and replication processes through its nuclease activity which initiates the resections of DNA ends in DNA double-stranded breaks (DSBs) for homology-directed recombination (HDR) (74). In addition to its role at DSBs, MRN associates with unperturbed replication fork as well as stalled replication forks (75-78). In particular, MRN complex is localized at telomeres during S phase through NBS1-TRF2 interaction (79,80). Moreover, MRN localizes to ALT-associated PML bodies (APBs) in ALT cells and is essential for ALT activity and the generation of T-circles, as shown by depletion of MRN using shRNA leads to a decrease in APBs and compromises these processes (81-83). However, depletion of MRE11 itself does not affect the generation of C-circles (37), although sequestrations of MRN complex by overexpressing Sp100 protein or ATRX protein dramatically reduces the C-circle levels (16,53,84,85). Further analysis is needed to clarify the specific mechanisms underlying these observations and their implications for telomere maintenance in ALT cells.

Here, our study demonstrated that inhibiting the nuclease activity of MRE11 results in an increase in the generation of C-rich ssDNAs and C-circles. These findings suggest that the nuclease activity of MRE11 plays a role in regulating the levels of C-rich ssDNAs and C-circles, potentially contributing to the resolution of higher-order structures, such as G-quadruplexes in lagging strands (Fig. 6; [1-a']) or 5' flap structures in Okazaki fragments (Fig. 6; [4-a']). Notably, yeast genetics showed that *mre11* and the mre11 nuclease mutant are synthetic lethal with *rad27* (yeast homolog of human FEN1) (86), even though in vitro

biochemistry experiments did not reveal preferential MRE11 nuclease activity for flap structures (87).

Additionally, our study demonstrated that depletion of DNA2 leads to an increase in the generation of C-rich ssDNAs and C-circles, consistent with previous reports that showed elevated C-circles and APBs upon DNA2 depletion (37,44,88). DNA2 plays a crucial role in resolving G-quadruplex structures in lagging strand telomeres, which likely contributes to the observed accumulation of C-rich ssDNAs upon DNA2 depletion (Fig. 6; [1-a']).

DNA2 also plays a crucial role in Okazaki fragment processing, particularly in the removal of flap structures (44,89). Recent structural studies have unveiled that DNA2 adopts a cylindrical shape with a tunnel through which ssDNA passes, and its nuclease domain is embedded within this tunnel (90). DNA2 efficiently trims ssDNA from the ssDNA end and preferentially processes long flaps (Fig. 6; [4-a']). This process relies on its interaction with RPA (Replication Protein A) (90). We propose that DNA2 depletion results in an increased presence of long flaps, which are partly processed by FEN1 or engaged in strand displacement by DNA polymerase delta. FEN1 nuclease may contribute to the generation of C-rich ssDNAs by cleaving the middle of 5' flap structures when long-flap structures are not adequately processed by DNA2 (Fig. 6; [4]). However, the contribution of FEN1-mediated cleavage in C-rich ssDNAs may not be substantial when the flaps are long and bound by RPA. Indeed, further study is essential to fully elucidate the precise mechanisms by which these enzymes coordinate their activities for Okazaki fragment processes in lagging strand, particularly at ALT telomeres.

C-rich ssDNAs are generated by strand displacement of lagging strands.

Our results indicate that the loss of ATRX is a crucial factor in the generation of C-rich ssDNAs, likely facilitated by the accumulations of G-quadruplex (G4) structures and G4-associated R-loops at telomeres. This is supported by FANCM depletion and RAD51AP1 KO data that R-loop formation may contribute to the generation of C-rich ssDNAs, possibly by exposing parental lagging strands that can be recognized by CST-PP complex (Fig. 6; [1]).

CST-PP complex has critical roles during telomere replication in particular lagging strands (32). Previous reports demonstrated that CST complex has a role in resolving G4 structures at telomeres as well as genome wide (91). Interestingly, CST complex is detected in APBs (69). Depletion of CST leads to replication defects in ALT cells, accompanied by decreases in T-circles and C-circles (69). We interpret that CST's priming activity in exposed gap or G4 structures in lagging strands is responsible for the generation of C-rich ssDNAs and C-circles. These primed Okazaki fragments, created by DNA polymerase alpha, are subsequently extended by DNA polymerase delta (Fig. 6; [2]).

In ALT cells, the interplay between polymerase delta's excessive strand displacement activity, along with BLM helicase and other associated factors, plays a crucial role in ALT telomere elongation through Break-Induced Replication. We propose that primed C-strand Okazaki fragments, initiated by the CST-PP (CTC1-STN1-TEN1-Polα-Primase) complex, undergo prolonged extension facilitated by DNA polymerase delta and BLM helicase, resulting in the formation of long flap structures (Fig. 6; [3]). The unique excessive strand displacement activity in ALT cells enables the complete displacement of downstream DNA, leading to the accumulation of C-rich single-stranded DNA (Fig. 6; [5]).

Further investigations into the mechanisms underlying this process could provide valuable insights into the complex interplay between ATRX, G-quadruplex structures, R-loops, CST, and BLM/POLD3, contributing to our understanding of ALT telomere maintenance.

Data Availability

For additional information and requests regarding resources or reagents, please direct your inquiries to the corresponding author, Dr. Jaewon Min (JM5092@cumc.columbia.edu). Dr. Min is responsible for handling and fulfilling these requests.

Acknowledgements

We thank members of the Telomere biology Lab (Min Lab) at Columbia University for their invaluable critiques, discussions, and protocols. We thank Drs. Eros Lazzerini Denchi (NIH/NCI), Alessandro Vindigni (Washington University), and David Clynes (Oxford) for providing U2OS BLM KO, U2OS PRIMPOL KO, and U2OS^{ATRX} cells. We also thank Drs. Robert Lu (CMRI), Greg Ira (Baylor College of Medicine), Justin W. Leung (UT Health San Antonio), Kurt Runge (Cleveland Clinic), Max E. Gottesman (Columbia), Jean Gautier (Columbia), and Shan Zha (Columbia) for their helpful discussion.

Author contributions*:* Conceptualization, J.M..; methodology, Junyeop L., and J.M.; investigation, Junyeop L., Jina L., E.J.S., and J.M.; writing – original draft, J.M.; writing –

review & editing, Junyeop L., R.J.O, A.C., and J.M.; funding acquisition, R.J.O., A.C., and J.M.; resources, A.T., R.J.O., A.C., and J.M.

Declaration of interests: The authors declare no competing interests.

Funding

This work was supported by the following NIH/NCI grants: CA207209 (R.J.O), CA262316 (R.J.O), CA197774 (A.C.), and CA245259 (J.M.).

References

1. Shay, J.W. and Wright, W.E. (2019) Telomeres and telomerase: three decades of progress. *Nat Rev Genet*, **20**, 299-309.
2. Bryan, T.M., Englezou, A., Dalla-Pozza, L., Dunham, M.A. and Reddel, R.R. (1997) Evidence for an alternative mechanism for maintaining telomere length in human tumors and tumor-derived cell lines. *Nat Med*, **3**, 1271-1274.
3. Lydeard, J.R., Jain, S., Yamaguchi, M. and Haber, J.E. (2007) Break-induced replication and telomerase-independent telomere maintenance require Pol32. *Nature*, **448**, 820-823.
4. Roumelioti, F.M., Sotiriou, S.K., Katsini, V., Chiourea, M., Halazonetis, T.D. and Gagos, S. (2016) Alternative lengthening of human telomeres is a conservative DNA replication process with features of break-induced replication. *EMBO Rep*, **17**, 1731-1737.
5. Dilley, R.L., Verma, P., Cho, N.W., Winters, H.D., Wondisford, A.R. and Greenberg, R.A. (2016) Break-induced telomere synthesis underlies alternative telomere maintenance. *Nature*, **539**, 54-58.
6. Min, J., Wright, W.E. and Shay, J.W. (2017) Alternative Lengthening of Telomeres Mediated by Mitotic DNA Synthesis Engages Break-Induced Replication Processes. *Mol Cell Biol*, **37**.
7. Cesare, A.J. and Reddel, R.R. (2010) Alternative lengthening of telomeres: models, mechanisms and implications. *Nat Rev Genet*, **11**, 319-330.
8. Cesare, A.J. and Griffith, J.D. (2004) Telomeric DNA in ALT cells is characterized by free telomeric circles and heterogeneous t-loops. *Mol Cell Biol*, **24**, 9948-9957.
9. Doksani, Y., Wu, J.Y., de Lange, T. and Zhuang, X. (2013) Super-resolution fluorescence imaging of telomeres reveals TRF2-dependent T-loop formation. *Cell*, **155**, 345-356.
10. Mazzucco, G., Huda, A., Galli, M., Piccini, D., Giannattasio, M., Pessina, F. and Doksani, Y. (2020) Telomere damage induces internal loops that generate telomeric circles. *Nat Commun*, **11**, 5297.
11. Zhang, T., Zhang, Z., Li, F., Hu, Q., Liu, H., Tang, M., Ma, W., Huang, J., Songyang, Z., Rong, Y. *et al.* (2017) Looping-out mechanism for resolution of replicative stress at telomeres. *EMBO Rep*, **18**, 1412-1428.
12. Pickett, H.A., Cesare, A.J., Johnston, R.L., Neumann, A.A. and Reddel, R.R. (2009) Control of telomere length by a trimming mechanism that involves generation of t-circles. *EMBO J*, **28**, 799-809.
13. Li, J.S., Miralles Fuste, J., Simavorian, T., Bartocci, C., Tsai, J., Karlseder, J. and Lazzerini Denchi, E. (2017) TZAP: A telomere-associated protein involved in telomere length control. *Science*, **355**, 638-641.
14. Pickett, H.A., Henson, J.D., Au, A.Y., Neumann, A.A. and Reddel, R.R. (2011) Normal mammalian cells negatively regulate telomere length by telomere trimming. *Hum Mol Genet*, **20**, 4684-4692.
15. Oganesian, L. and Karlseder, J. (2013) 5' C-rich telomeric overhangs are an outcome of rapid telomere truncation events. *DNA Repair (Amst)*, **12**, 238-245.
16. Henson, J.D., Cao, Y., Huschtscha, L.I., Chang, A.C., Au, A.Y., Pickett, H.A. and Reddel, R.R. (2009) DNA C-circles are specific and quantifiable markers of alternative-lengthening-of-telomeres activity. *Nat Biotechnol*, **27**, 1181-1185.
17. Idilli, A.I., Segura-Bayona, S., Lippert, T.P. and Boulton, S.J. (2021) A C-circle assay for detection of alternative lengthening of telomere activity in FFPE tissue. *STAR Protoc*, **2**, 100569.
18. Chen, Y.Y., Dagg, R., Zhang, Y., Lee, J.H.Y., Lu, R., Martin La Rotta, N., Sampl, S., Korkut-Demirbas, M., Holzmann, K., Lau, L.M.S. *et al.* (2021) The C-Circle Biomarker Is Secreted by Alternative-Lengthening-of-Telomeres Positive Cancer Cells inside Exosomes and Provides a Blood-Based Diagnostic for ALT Activity. *Cancers (Basel)*, **13**.

19. Henson, J.D., Lau, L.M., Koch, S., Martin La Rotta, N., Dagg, R.A. and Reddel, R.R. (2017) The C-Circle Assay for alternative-lengthening-of-telomeres activity. *Methods*, **114**, 74-84.
20. Jones, C.Y., Williams, C.L., Moreno, S.P., Morris, D.K., Mondello, C., Karlseder, J. and Bertuch, A.A. (2023) Hyperextended telomeres promote formation of C-circle DNA in telomerase positive human cells. *J Biol Chem*, **299**, 104665.
21. Min, J., Wright, W.E. and Shay, J.W. (2017) Alternative lengthening of telomeres can be maintained by preferential elongation of lagging strands. *Nucleic Acids Res*, **45**, 2615-2628.
22. Zhang, T., Zhang, Z., Shengzhao, G., Li, X., Liu, H. and Zhao, Y. (2019) Strand break-induced replication fork collapse leads to C-circles, C-overhangs and telomeric recombination. *PLoS Genet*, **15**, e1007925.
23. Lu, R. and Pickett, H.A. (2022) Telomeric replication stress: the beginning and the end for alternative lengthening of telomeres cancers. *Open Biol*, **12**, 220011.
24. Nabetani, A. and Ishikawa, F. (2009) Unusual telomeric DNAs in human telomerase-negative immortalized cells. *Mol Cell Biol*, **29**, 703-713.
25. Oganesian, L. and Karlseder, J. (2011) Mammalian 5' C-rich telomeric overhangs are a mark of recombination-dependent telomere maintenance. *Mol Cell*, **42**, 224-236.
26. Zhang, T., Rawal, Y., Jiang, H., Kwon, Y., Sung, P. and Greenberg, R.A. (2023) Break-induced replication orchestrates resection-dependent template switching. *Nature*, **619**, 201-208.
27. Emam, A., Wu, X., Xu, S., Wang, L., Liu, S. and Wang, B. (2022) Stalled replication fork protection limits cGAS-STING and P-body-dependent innate immune signalling. *Nat Cell Biol*, **24**, 1154-1164.
28. Cheng, I.-C., Chen, B.C., Shuai, H.-H., Chien, F.-C., Chen, P. and Hsieh, T.-s. (2016) Wuho is a new member in maintaining genome stability through its interaction with flap endonuclease 1. *PLoS biology*, **14**, e1002349.
29. Taglialatela, A., Leuzzi, G., Sannino, V., Cuella-Martin, R., Huang, J.W., Wu-Baer, F., Baer, R., Costanzo, V. and Ciccia, A. (2021) REV1-Polzeta maintains the viability of homologous recombination-deficient cancer cells through mutagenic repair of PRIMPOL-dependent ssDNA gaps. *Mol Cell*, **81**, 4008-4025 e4007.
30. Pan, X., Chen, Y., Biju, B., Ahmed, N., Kong, J., Goldenberg, M., Huang, J., Mohan, N., Klosek, S., Parsa, K. *et al.* (2019) FANCM suppresses DNA replication stress at ALT telomeres by disrupting TERRA R-loops. *Sci Rep*, **9**, 19110.
31. Li, S., Wang, H., Jehi, S., Li, J., Liu, S., Wang, Z., Truong, L., Chiba, T., Wang, Z. and Wu, X. (2021) PIF1 helicase promotes break-induced replication in mammalian cells. *EMBO J*, **40**, e104509.
32. Huang, C., Dai, X. and Chai, W. (2012) Human Stn1 protects telomere integrity by promoting efficient lagging-strand synthesis at telomeres and mediating C-strand fill-in. *Cell Res*, **22**, 1681-1695.
33. Lovejoy, C.A., Li, W., Reisenweber, S., Thongthip, S., Bruno, J., de Lange, T., De, S., Petrini, J.H., Sung, P.A., Jasin, M. *et al.* (2012) Loss of ATRX, genome instability, and an altered DNA damage response are hallmarks of the alternative lengthening of telomeres pathway. *PLoS Genet*, **8**, e1002772.
34. Lai, T.P., Wright, W.E. and Shay, J.W. (2016) Generation of digoxigenin-incorporated probes to enhance DNA detection sensitivity. *Biotechniques*, **60**, 306-309.
35. Kim, Y.K., Yeo, J., Kim, B., Ha, M. and Kim, V.N. (2012) Short structured RNAs with low GC content are selectively lost during extraction from a small number of cells. *Mol Cell*, **46**, 893-895.
36. Dupre, A., Boyer-Chatenet, L., Sattler, R.M., Modi, A.P., Lee, J.H., Nicolette, M.L., Kopelovich, L., Jasin, M., Baer, R., Paull, T.T. *et al.* (2008) A forward chemical genetic screen reveals an inhibitor of the Mre11-Rad50-Nbs1 complex. *Nat Chem Biol*, **4**, 119-125.
37. O'Sullivan, R.J., Arnoult, N., Lackner, D.H., Oganesian, L., Haggblom, C., Corpet, A., Almouzni, G. and Karlseder, J. (2014) Rapid induction of alternative lengthening of telomeres by depletion of the histone chaperone ASF1. *Nat Struct Mol Biol*, **21**, 167-174.

38. Shibata, A., Moiani, D., Arvai, A.S., Perry, J., Harding, S.M., Genois, M.M., Maity, R., van Rossum-Fikkert, S., Kertokalio, A., Romoli, F. *et al.* (2014) DNA double-strand break repair pathway choice is directed by distinct MRE11 nuclease activities. *Mol Cell*, **53**, 7-18.
39. Arnoult, N., Saintome, C., Ourliac-Garnier, I., Riou, J.F. and Londono-Vallejo, A. (2009) Human POT1 is required for efficient telomere C-rich strand replication in the absence of WRN. *Genes Dev*, **23**, 2915-2924.
40. Zimmer, J., Tacconi, E.M.C., Folio, C., Badie, S., Porru, M., Klare, K., Tumiati, M., Markkanen, E., Halder, S., Ryan, A. *et al.* (2016) Targeting BRCA1 and BRCA2 Deficiencies with G-Quadruplex-Interacting Compounds. *Mol Cell*, **61**, 449-460.
41. Zimmermann, M., Kibe, T., Kabir, S. and de Lange, T. (2014) TRF1 negotiates TTAGGG repeat-associated replication problems by recruiting the BLM helicase and the TPP1/POT1 repressor of ATR signaling. *Genes Dev*, **28**, 2477-2491.
42. Lee, J., Sung, K., Joo, S.Y., Jeong, J.H., Kim, S.K. and Lee, H. (2022) Dynamic interaction of BRCA2 with telomeric G-quadruplexes underlies telomere replication homeostasis. *Nat Commun*, **13**, 3396.
43. Lin, W., Sampathi, S., Dai, H., Liu, C., Zhou, M., Hu, J., Huang, Q., Campbell, J., Shin-Ya, K., Zheng, L. *et al.* (2013) Mammalian DNA2 helicase/nuclease cleaves G-quadruplex DNA and is required for telomere integrity. *EMBO J*, **32**, 1425-1439.
44. Sun, H., Ma, L., Tsai, Y.F., Abeywardana, T., Shen, B. and Zheng, L. (2023) Okazaki fragment maturation: DNA flap dynamics for cell proliferation and survival. *Trends Cell Biol*, **33**, 221-234.
45. Hanzlikova, H., Kalasova, I., Demin, A.A., Pennicott, L.E., Cihlarova, Z. and Caldecott, K.W. (2018) The Importance of Poly(ADP-Ribose) Polymerase as a Sensor of Unligated Okazaki Fragments during DNA Replication. *Mol Cell*, **71**, 319-331 e313.
46. Cong, K., Peng, M., Kousholt, A.N., Lee, W.T.C., Lee, S., Nayak, S., Krais, J., VanderVere-Carozza, P.S., Pawelczak, K.S., Calvo, J. *et al.* (2021) Replication gaps are a key determinant of PARP inhibitor synthetic lethality with BRCA deficiency. *Mol Cell*, **81**, 3128-3144 e3127.
47. Shen, Y., Rehman, F.L., Feng, Y., Boshuizen, J., Bajrami, I., Elliott, R., Wang, B., Lord, C.J., Post, L.E. and Ashworth, A. (2013) BMN 673, a novel and highly potent PARP1/2 inhibitor for the treatment of human cancers with DNA repair deficiency. *Clin Cancer Res*, **19**, 5003-5015.
48. Garcia-Gomez, S., Reyes, A., Martinez-Jimenez, M.I., Chocron, E.S., Mouron, S., Terrados, G., Powell, C., Salido, E., Mendez, J., Holt, I.J. *et al.* (2013) PrimPol, an archaic primase/polymerase operating in human cells. *Mol Cell*, **52**, 541-553.
49. Tirman, S., Quinet, A., Wood, M., Meroni, A., Cybulla, E., Jackson, J., Pegoraro, S., Simoneau, A., Zou, L. and Vindigni, A. (2021) Temporally distinct post-replicative repair mechanisms fill PRIMPOL-dependent ssDNA gaps in human cells. *Mol Cell*, **81**, 4026-4040 e4028.
50. Quinet, A., Tirman, S., Jackson, J., Svikovic, S., Lemacon, D., Carvajal-Maldonado, D., Gonzalez-Acosta, D., Vessoni, A.T., Cybulla, E., Wood, M. *et al.* (2020) PRIMPOL-Mediated Adaptive Response Suppresses Replication Fork Reversal in BRCA-Deficient Cells. *Mol Cell*, **77**, 461-474 e469.
51. Mehta, K.P.M., Thada, V., Zhao, R., Krishnamoorthy, A., Leser, M., Lindsey Rose, K. and Cortez, D. (2022) CHK1 phosphorylates PRIMPOL to promote replication stress tolerance. *Sci Adv*, **8**, eabm0314.
52. Heaphy, C.M., de Wilde, R.F., Jiao, Y., Klein, A.P., Edil, B.H., Shi, C., Bettegowda, C., Rodriguez, F.J., Eberhart, C.G., Hebbar, S. *et al.* (2011) Altered telomeres in tumors with ATRX and DAXX mutations. *Science*, **333**, 425.
53. Clynes, D., Jelinska, C., Xella, B., Ayyub, H., Scott, C., Mitson, M., Taylor, S., Higgs, D.R. and Gibbons, R.J. (2015) Suppression of the alternative lengthening of telomere pathway by the chromatin remodelling factor ATRX. *Nat Commun*, **6**, 7538.

54. Nguyen, D.T., Voon, H.P.J., Xella, B., Scott, C., Clynes, D., Babbs, C., Ayyub, H., Kerry, J., Sharpe, J.A., Sloane-Stanley, J.A. *et al.* (2017) The chromatin remodelling factor ATRX suppresses R-loops in transcribed telomeric repeats. *EMBO Rep*, **18**, 914-928.
55. Teng, Y.C., Sundaresan, A., O'Hara, R., Gant, V.U., Li, M., Martire, S., Warshaw, J.N., Basu, A. and Banaszynski, L.A. (2021) ATRX promotes heterochromatin formation to protect cells from G-quadruplex DNA-mediated stress. *Nat Commun*, **12**, 3887.
56. Silva, B., Pentz, R., Figueira, A.M., Arora, R., Lee, Y.W., Hodson, C., Wischnewski, H., Deans, A.J. and Azzalin, C.M. (2019) FANCM limits ALT activity by restricting telomeric replication stress induced by deregulated BLM and R-loops. *Nat Commun*, **10**, 2253.
57. Lu, R., O'Rourke, J.J., Sobinoff, A.P., Allen, J.A.M., Nelson, C.B., Tomlinson, C.G., Lee, M., Reddel, R.R., Deans, A.J. and Pickett, H.A. (2019) The FANCM-BLM-TOP3A-RMI complex suppresses alternative lengthening of telomeres (ALT). *Nat Commun*, **10**, 2252.
58. Barroso-Gonzalez, J., Garcia-Exposito, L., Hoang, S.M., Lynskey, M.L., Roncaioli, J.L., Ghosh, A., Wallace, C.T., de Vitis, M., Modesti, M., Bernstein, K.A. *et al.* (2019) RAD51AP1 Is an Essential Mediator of Alternative Lengthening of Telomeres. *Mol Cell*, **76**, 11-26 e17.
59. Decottignies, A. (2022) TERRA and RAD51AP1 at the R&D-loop department of ALT telomeres. *Mol Cell*, **82**, 3963-3965.
60. Yadav, T., Zhang, J.M., Ouyang, J., Leung, W., Simoneau, A. and Zou, L. (2022) TERRA and RAD51AP1 promote alternative lengthening of telomeres through an R- to D-loop switch. *Mol Cell*, **82**, 3985-4000 e3984.
61. Kaminski, N., Wondisford, A.R., Kwon, Y., Lynskey, M.L., Bhargava, R., Barroso-Gonzalez, J., Garcia-Exposito, L., He, B., Xu, M., Mellacheruvu, D. *et al.* (2022) RAD51AP1 regulates ALT-HDR through chromatin-directed homeostasis of TERRA. *Mol Cell*, **82**, 4001-4017 e4007.
62. Lovejoy, C.A., Takai, K., Huh, M.S., Picketts, D.J. and de Lange, T. (2020) ATRX affects the repair of telomeric DSBs by promoting cohesion and a DAXX-dependent activity. *PLoS Biol*, **18**, e3000594.
63. Geiller, H.E.B., Harvey, A., Jones, R.E., Grimstead, J.W., Cleal, K., Hendrickson, E.A. and Baird, D.M. (2022) ATRX modulates the escape from a telomere crisis. *PLoS Genet*, **18**, e1010485.
64. Napier, C.E., Huschtscha, L.I., Harvey, A., Bower, K., Noble, J.R., Hendrickson, E.A. and Reddel, R.R. (2015) ATRX represses alternative lengthening of telomeres. *Oncotarget*, **6**, 16543-16558.
65. Cai, S.W. and de Lange, T. (2023) CST-Polalpha/Primase: the second telomere maintenance machine. *Genes Dev*.
66. Zhang, M., Wang, B., Li, T., Liu, R., Xiao, Y., Geng, X., Li, G., Liu, Q., Price, C.M., Liu, Y. *et al.* (2019) Mammalian CST averts replication failure by preventing G-quadruplex accumulation. *Nucleic Acids Res*, **47**, 5243-5259.
67. Miyake, Y., Nakamura, M., Nabetani, A., Shimamura, S., Tamura, M., Yonehara, S., Saito, M. and Ishikawa, F. (2009) RPA-like mammalian Ctc1-Stn1-Ten1 complex binds to single-stranded DNA and protects telomeres independently of the Pot1 pathway. *Mol Cell*, **36**, 193-206.
68. Wang, F., Stewart, J.A., Kasbek, C., Zhao, Y., Wright, W.E. and Price, C.M. (2012) Human CST has independent functions during telomere duplex replication and C-strand fill-in. *Cell Rep*, **2**, 1096-1103.
69. Huang, C., Jia, P., Chastain, M., Shiva, O. and Chai, W. (2017) The human CTC1/STN1/TEN1 complex regulates telomere maintenance in ALT cancer cells. *Exp Cell Res*, **355**, 95-104.
70. Min, J., Wright, W.E. and Shay, J.W. (2019) Clustered telomeres in phase-separated nuclear condensates engage mitotic DNA synthesis through BLM and RAD52. *Genes Dev*, **33**, 814-827.
71. Sobinoff, A.P., Allen, J.A., Neumann, A.A., Yang, S.F., Walsh, M.E., Henson, J.D., Reddel, R.R. and Pickett, H.A. (2017) BLM and SLX4 play opposing roles in recombination-dependent replication at human telomeres. *EMBO J*, **36**, 2907-2919.

72. Loe, T.K., Li, J.S.Z., Zhang, Y., Azeroglu, B., Boddy, M.N. and Denchi, E.L. (2020) Telomere length heterogeneity in ALT cells is maintained by PML-dependent localization of the BTR complex to telomeres. *Genes Dev*, **34**, 650-662.
73. Min, J., Zhao, J., Zagelbaum, J., Lee, J., Takahashi, S., Cummings, P., Schooley, A., Dekker, J., Gottesman, M.E., Rabadan, R. *et al.* (2023) Mechanisms of insertions at a DNA double-strand break. *Mol Cell*.
74. Symington, L.S. and Gautier, J. (2011) Double-strand break end resection and repair pathway choice. *Annu Rev Genet*, **45**, 247-271.
75. Oh, J. and Symington, L.S. (2018) Role of the Mre11 Complex in Preserving Genome Integrity. *Genes (Basel)*, **9**.
76. Costanzo, V., Robertson, K., Bibikova, M., Kim, E., Grieco, D., Gottesman, M., Carroll, D. and Gautier, J. (2001) Mre11 protein complex prevents double-strand break accumulation during chromosomal DNA replication. *Mol Cell*, **8**, 137-147.
77. Sirbu, B.M., Couch, F.B., Feigerle, J.T., Bhaskara, S., Hiebert, S.W. and Cortez, D. (2011) Analysis of protein dynamics at active, stalled, and collapsed replication forks. *Genes Dev*, **25**, 1320-1327.
78. Maser, R.S., Mirzoeva, O.K., Wells, J., Olivares, H., Williams, B.R., Zinkel, R.A., Farnham, P.J. and Petrini, J.H. (2001) Mre11 complex and DNA replication: linkage to E2F and sites of DNA synthesis. *Mol Cell Biol*, **21**, 6006-6016.
79. Rai, R., Hu, C., Broton, C., Chen, Y., Lei, M. and Chang, S. (2017) NBS1 Phosphorylation Status Dictates Repair Choice of Dysfunctional Telomeres. *Mol Cell*, **65**, 801-817 e804.
80. Zhu, X.D., Kuster, B., Mann, M., Petrini, J.H. and de Lange, T. (2000) Cell-cycle-regulated association of RAD50/MRE11/NBS1 with TRF2 and human telomeres. *Nat Genet*, **25**, 347-352.
81. Compton, S.A., Choi, J.H., Cesare, A.J., Ozgur, S. and Griffith, J.D. (2007) Xrcc3 and Nbs1 are required for the production of extrachromosomal telomeric circles in human alternative lengthening of telomere cells. *Cancer Res*, **67**, 1513-1519.
82. Zhong, Z.H., Jiang, W.Q., Cesare, A.J., Neumann, A.A., Wadhwa, R. and Reddel, R.R. (2007) Disruption of telomere maintenance by depletion of the MRE11/RAD50/NBS1 complex in cells that use alternative lengthening of telomeres. *J Biol Chem*, **282**, 29314-29322.
83. Yu, E.Y., Perez-Martin, J., Holloman, W.K. and Lue, N.F. (2015) Mre11 and Blm-Dependent Formation of ALT-Like Telomeres in Ku-Deficient Ustilago maydis. *PLoS Genet*, **11**, e1005570.
84. Jiang, W.Q., Zhong, Z.H., Henson, J.D., Neumann, A.A., Chang, A.C. and Reddel, R.R. (2005) Suppression of alternative lengthening of telomeres by Sp100-mediated sequestration of the MRE11/RAD50/NBS1 complex. *Mol Cell Biol*, **25**, 2708-2721.
85. Leung, J.W., Ghosal, G., Wang, W., Shen, X., Wang, J., Li, L. and Chen, J. (2013) Alpha thalassemia/mental retardation syndrome X-linked gene product ATRX is required for proper replication restart and cellular resistance to replication stress. *J Biol Chem*, **288**, 6342-6350.
86. Moreau, S., Ferguson, J.R. and Symington, L.S. (1999) The nuclease activity of Mre11 is required for meiosis but not for mating type switching, end joining, or telomere maintenance. *Mol Cell Biol*, **19**, 556-566.
87. Paull, T.T. and Gellert, M. (1998) The 3' to 5' exonuclease activity of Mre 11 facilitates repair of DNA double-strand breaks. *Mol Cell*, **1**, 969-979.
88. Panier, S., Maric, M., Hewitt, G., Mason-Osann, E., Gali, H., Dai, A., Labadorf, A., Guervilly, J.H., Ruis, P., Segura-Bayona, S. *et al.* (2019) SLX4IP Antagonizes Promiscuous BLM Activity during ALT Maintenance. *Mol Cell*, **76**, 27-43 e11.
89. Yu, Y., Pham, N., Xia, B., Papusha, A., Wang, G., Yan, Z., Peng, G., Chen, K. and Ira, G. (2018) Dna2 nuclease deficiency results in large and complex DNA insertions at chromosomal breaks. *Nature*, **564**, 287-290.

90. Zhou, C., Pourmal, S. and Pavletich, N.P. (2015) Dna2 nuclease-helicase structure, mechanism and regulation by Rpa. *Elife*, **4**.
91. Li, T., Zhang, M., Li, Y., Han, X., Tang, L., Ma, T., Zhao, X., Zhao, R., Wang, Y., Bai, X. *et al.* (2023) Cooperative interaction of CST and RECQ4 resolves G-quadruplexes and maintains telomere stability. *EMBO Rep*, e55494.

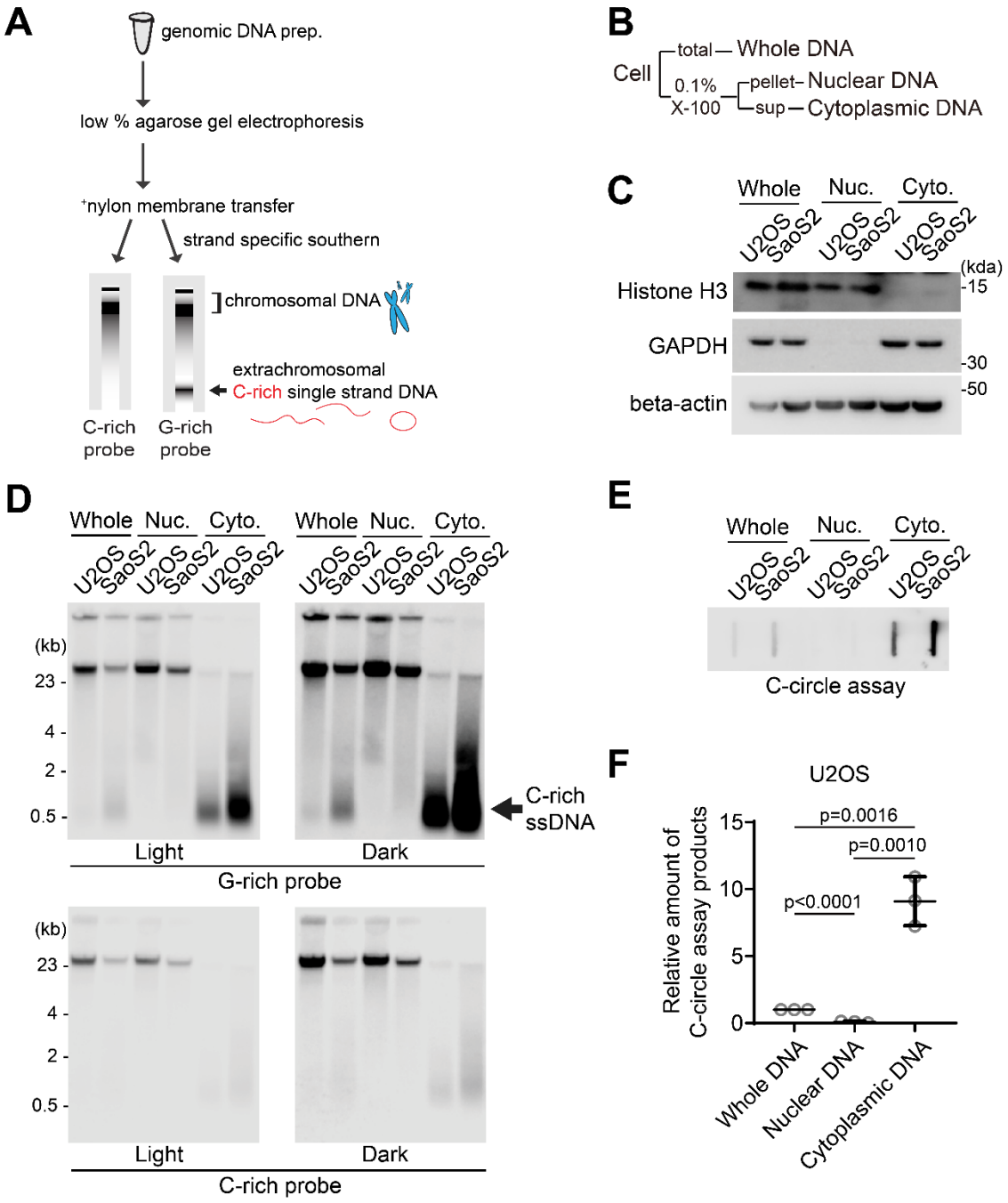

Figure 1. Enrichment of extrachromosomal telomeres in cytoplasm. (A) Illustration of the Strand-specific Southern for Single Stranded Extrachromosomal Telomeres (4SET) method. (Refer to the text for details) **(B)** The 4SET method involves the fractionation of samples into Whole DNA fraction, Nuclear DNA fraction, and Cytoplasmic DNA fraction, achieved using 0.1% Triton X-100. **(C)** Western blot analysis of the Whole, Nuclear, and Cytoplasmic fractions using anti-Histone H3, GAPDH, and beta-actin for the validation of cell fractions. **(D)** 4SET assay for U2OS and SaoS2 cells after fractionation of samples into Whole, Nuclear, and Cytoplasmic DNA fractions. G-rich probe was used to detect C-rich telomeric sequences, and C-rich probe was used to detect G-rich telomeric sequences. C-rich single stranded DNAs are indicated by an arrow. **(E)** C-circle assay for U2OS and SaoS2 cells after fractionation of samples into Whole, Nuclear, and Cytoplasmic DNA fractions. **(F)** Quantification of the C-circle assay in E; U2OS cells as the relative amount of C-circle assay products (mean ± SD; unpaired t-test).

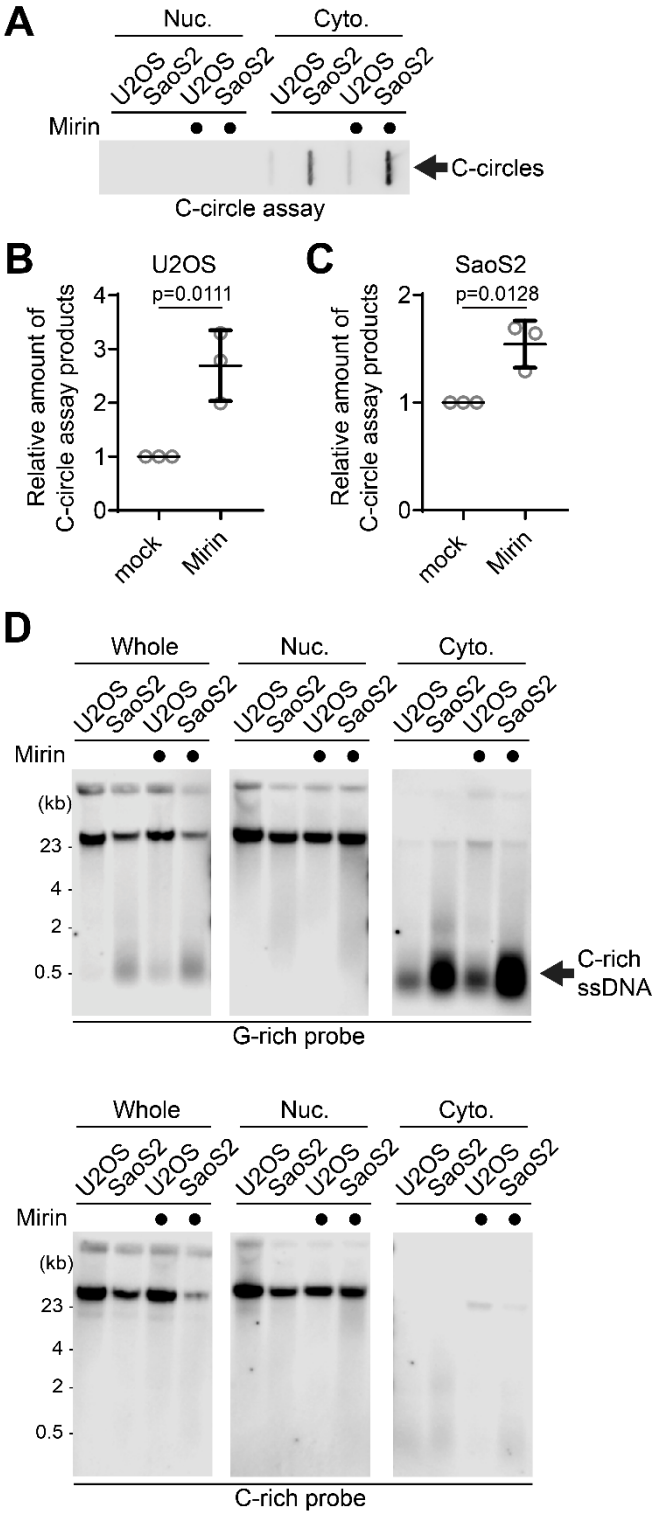

Figure 2. MRE11 nuclease inhibition leads to increases in C-circles and C-rich ssDNAs. (A) C-circle assay for U2OS and SaoS2 cells with or without Mirin (MRE11 nuclease inhibitor) treatment. Samples were fractionated into nuclear, and cytoplasmic DNA fractions. U2OS and Saos2 cells were treated with 50 μM Mirin for 48 hr. **(B-C)** Quantification of the C-circle assay in A; U2OS cells (B), and SaoS2 cells (C), as the relative amount of C-circle assay products (mean ± SD; unpaired t-test). **(D)** 4SET assay for U2OS and SaoS2 cells with or without Mirin treatment after fractionation of samples into Whole, Nuclear, and Cytoplasmic DNA fractions. G-rich probe was used to detect C-rich telomeric sequences, and C-rich probe was used to detect G-rich telomeric sequences. C-rich single stranded DNAs are indicated by an arrow.

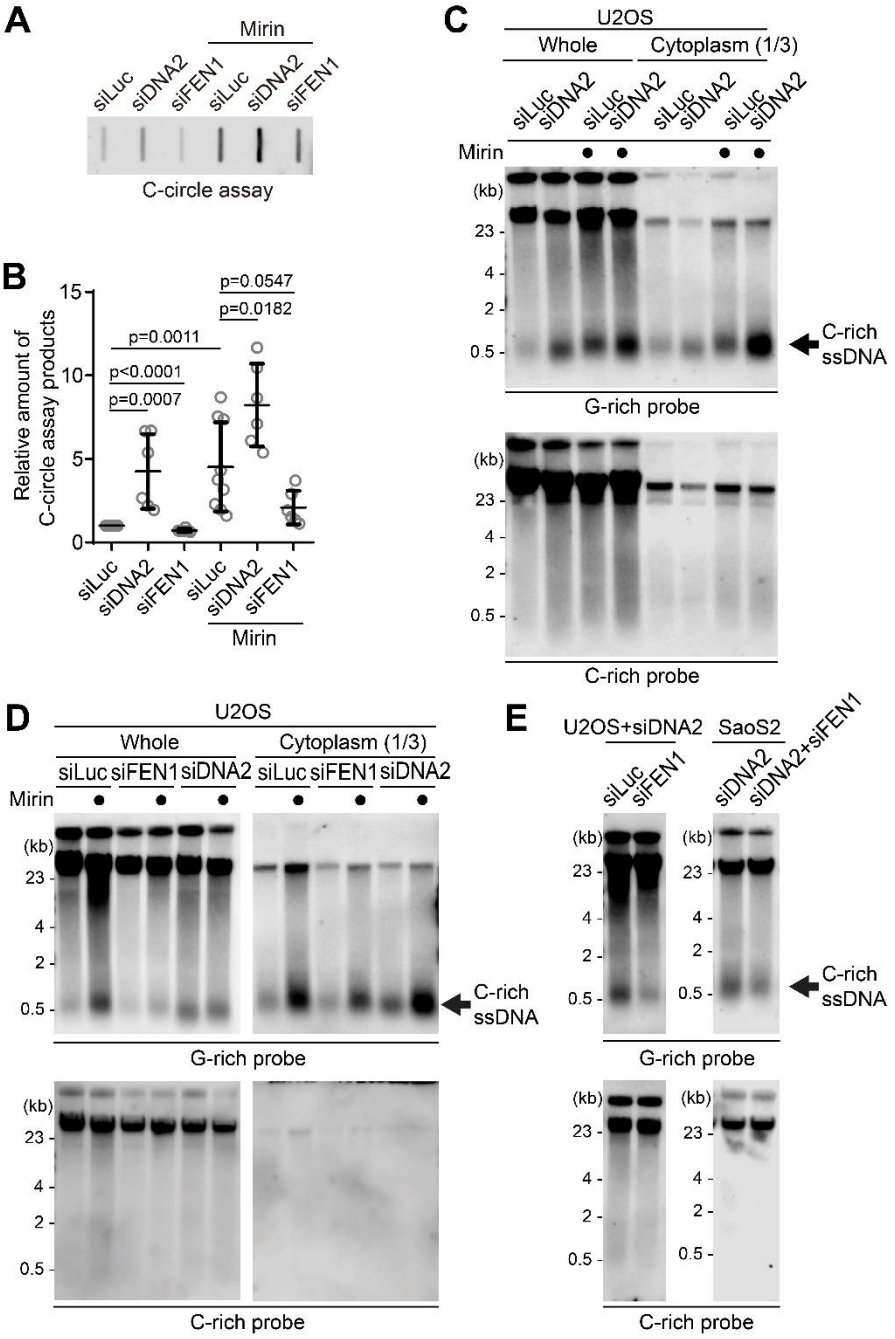

Figure 3. C-circles and C-rich ssDNAs are generated during Okazaki fragment processing. (A) C-circle assay for U2OS cells after transfection of siRNAs targeting DNA2 or FEN1 with or without Mirin treatment. **(B)** Quantification of the C-circle assay in A as the relative amount of C-circle assay products (mean ± SD; unpaired t-test). **(C)** 4SET assay for U2OS cells after transfection of siRNAs targeting DNA2, or control (siLuc) with or without Mirin treatment. Samples were fractionated into cytoplasmic DNA fraction or whole DNA. G-rich probe was used to detect C-rich telomeric sequences, and C-rich probe was used to detect G-rich telomeric sequences. C-rich single stranded DNAs are indicated by an arrow. **(D)** 4SET assay for U2OS cells after transfection of siRNAs targeting FEN1, DNA2, or control (siLuc) with or without Mirin treatment. Samples were fractionated into cytoplasmic DNA fraction or whole DNA. G-rich probe was used to detect C-rich telomeric sequences, and C-rich probe was used to detect G-rich telomeric sequences. C-rich single stranded DNAs are indicated by an arrow. **(E)** 4SET assay for U2OS and SaoS2 cells after transfection of siRNAs targeting FEN1 and DNA2, or DNA2 alone. G-rich probe was used to detect C-rich telomeric sequences, and C-rich probe was used to detect G-rich telomeric sequences. C-rich single stranded DNAs are indicated by an arrow.

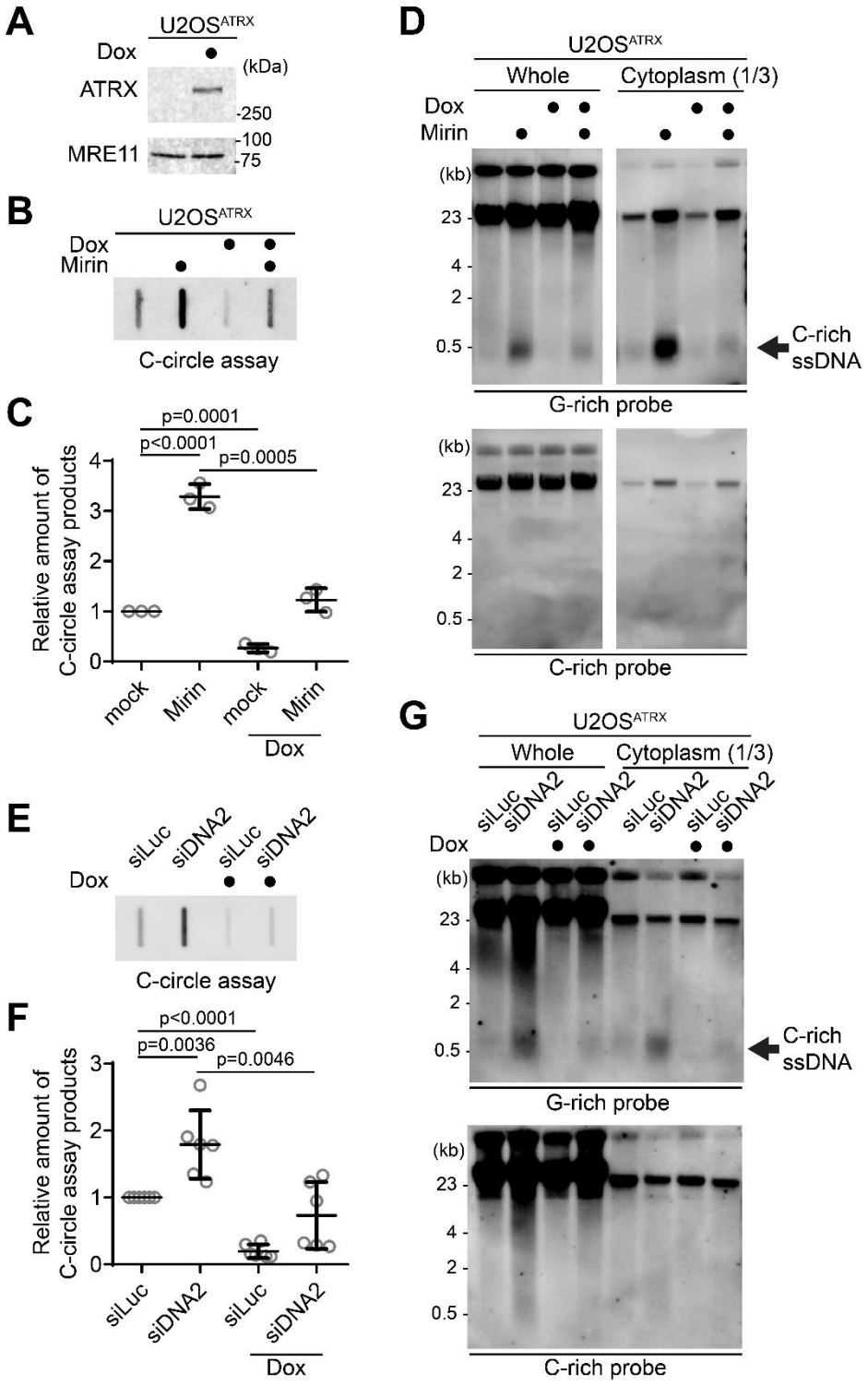

Figure 4. ATRX suppresses the C-rich ssDNA generation. (A) Western blot analysis of U2OS^{ATRX} cells with ectopic ATRX expression under a doxycycline-inducible promoter, using anti-ATRX and MRE11 antibodies for the validation of ATRX expression and MRE11 levels, respectively. **(B)** C-circle assay for U2OS^{ATRX} cells treated with doxycycline for one week or left untreated, with or without Mirin treatment (50 μM Mirin for 48 hr). **(C)** Quantification of the C-circle assay in B as the relative amount of C-circle assay products (mean ± SD; unpaired t-test). **(D)** 4SET assay for U2OS^{ATRX} cells treated with doxycycline for one week or left untreated, with or without Mirin treatment (50 μM Mirin for 48 hr). Samples were fractionated into cytoplasmic DNA fraction or whole DNA. G-rich probe was used to detect C-rich telomeric sequences, and C-rich probe was used to detect G-rich telomeric sequences.

C-rich single stranded DNAs are indicated by an arrow. **(E)** C-circle assay for U2OS^{ATRX} cells treated with doxycycline for one week or left untreated. Cells were transfected with siRNAs targeting DNA2, or control (siLuc). **(F)** Quantification of the C-circle assay in B as the relative amount of C-circle assay products (mean ± SD; unpaired t-test). **(G)** 4SET assay for U2OS^{ATRX} cells treated with doxycycline for one week or left untreated. Cells were transfected with siRNAs targeting DNA2, or control (siLuc). Samples were fractionated into cytoplasmic DNA fraction or whole DNA. G-rich probe was used to detect C-rich telomeric sequences, and C-rich probe was used to detect G-rich telomeric sequences. C-rich single stranded DNAs are indicated by an arrow.

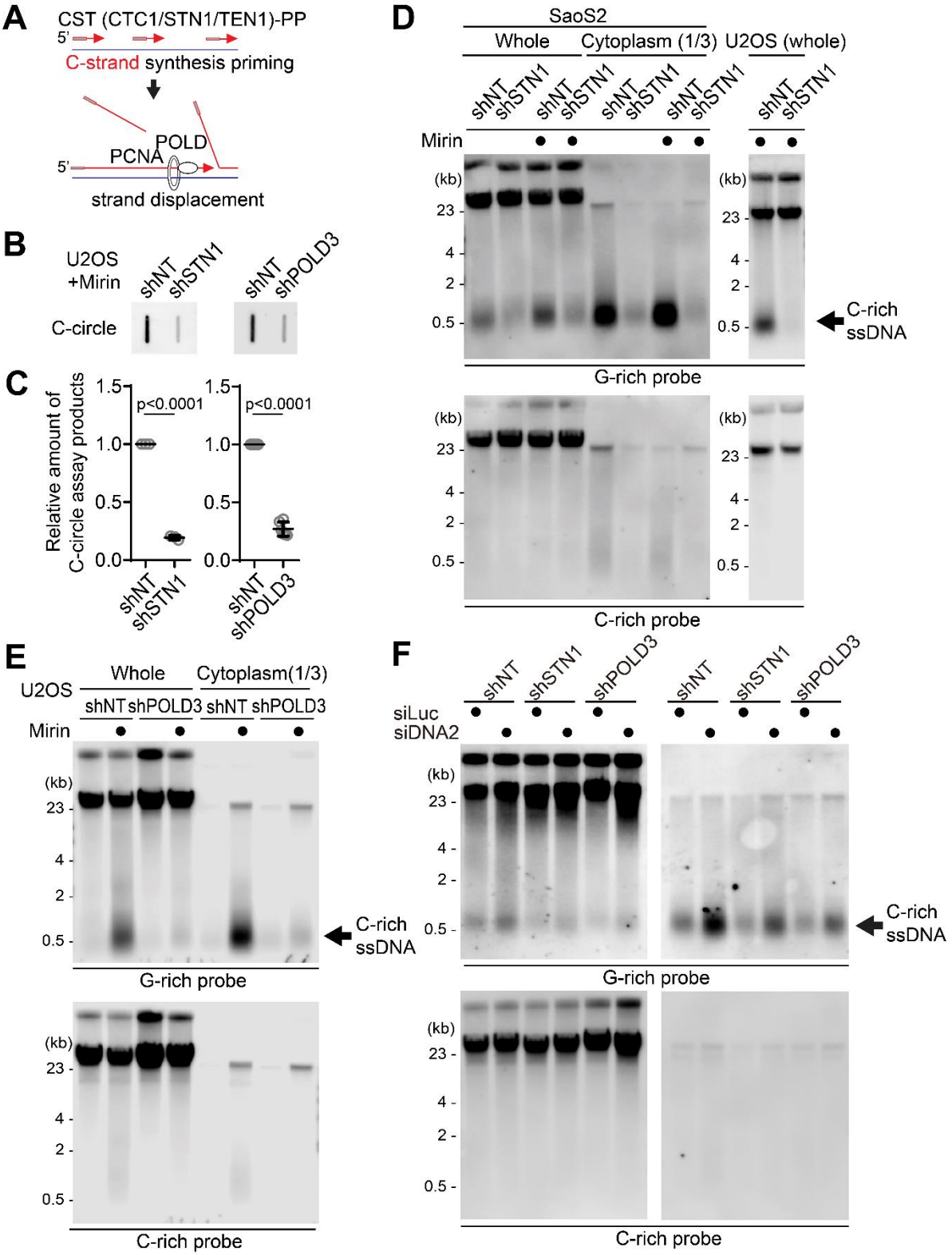

Figure 5. **C-circles and C-rich ssDNAs are generated through C-strand priming and subsequent strand displacement. (A)** Illustration depicting C-strand synthesis priming by CST-PP (CTC1/STN1/TEN1-Primase-Polymerase alpha)-complex and the strand displacement of Okazaki fragments by PCNA and DNA polymerase delta (POLD) during DNA replication on the lagging strand. **(B)** C-circle assay for U2OS cells expressing shRNAs targeting STN1, POLD3, or non-targeting (NT) control. Cells were treated with Mirin (50 μM, 48 hr) **(C)** Quantification of the C-circle assay in B as the relative amount of C-circle assay products (mean ± SD; unpaired t-test). **(D)** 4SET assay for SaoS2

and U2OS cells expressing shRNAs targeting STN1, or non-targeting (NT) control. Cells were treated with Mirin (50 μM, 48 hr). Samples were fractionated into cytoplasmic DNA fraction or whole DNA. G-rich probe was used to detect C-rich telomeric sequences, and C-rich probe was used to detect G-rich telomeric sequences. C-rich single stranded DNAs are indicated by an arrow. **(E)** 4SET assay for U2OS cells expressing shRNAs targeting POLD3, or non-targeting (NT) control. Samples were fractionated into cytoplasmic DNA fraction or whole DNA. G-rich probe was used to detect C-rich telomeric sequences, and C-rich probe was used to detect G-rich telomeric sequences. C-rich single stranded DNAs are indicated by an arrow. **(E)** 4SET assay for U2OS cells expressing shRNAs targeting STN1, POLD3, or non-targeting (NT) control after transfection of siRNAs targeting DNA2 or control (siLuc). Samples were fractionated into cytoplasmic DNA fraction or whole DNA. G-rich probe was used to detect C-rich telomeric sequences, and C-rich probe was used to detect G-rich telomeric sequences. C-rich single stranded DNAs are indicated by an arrow.

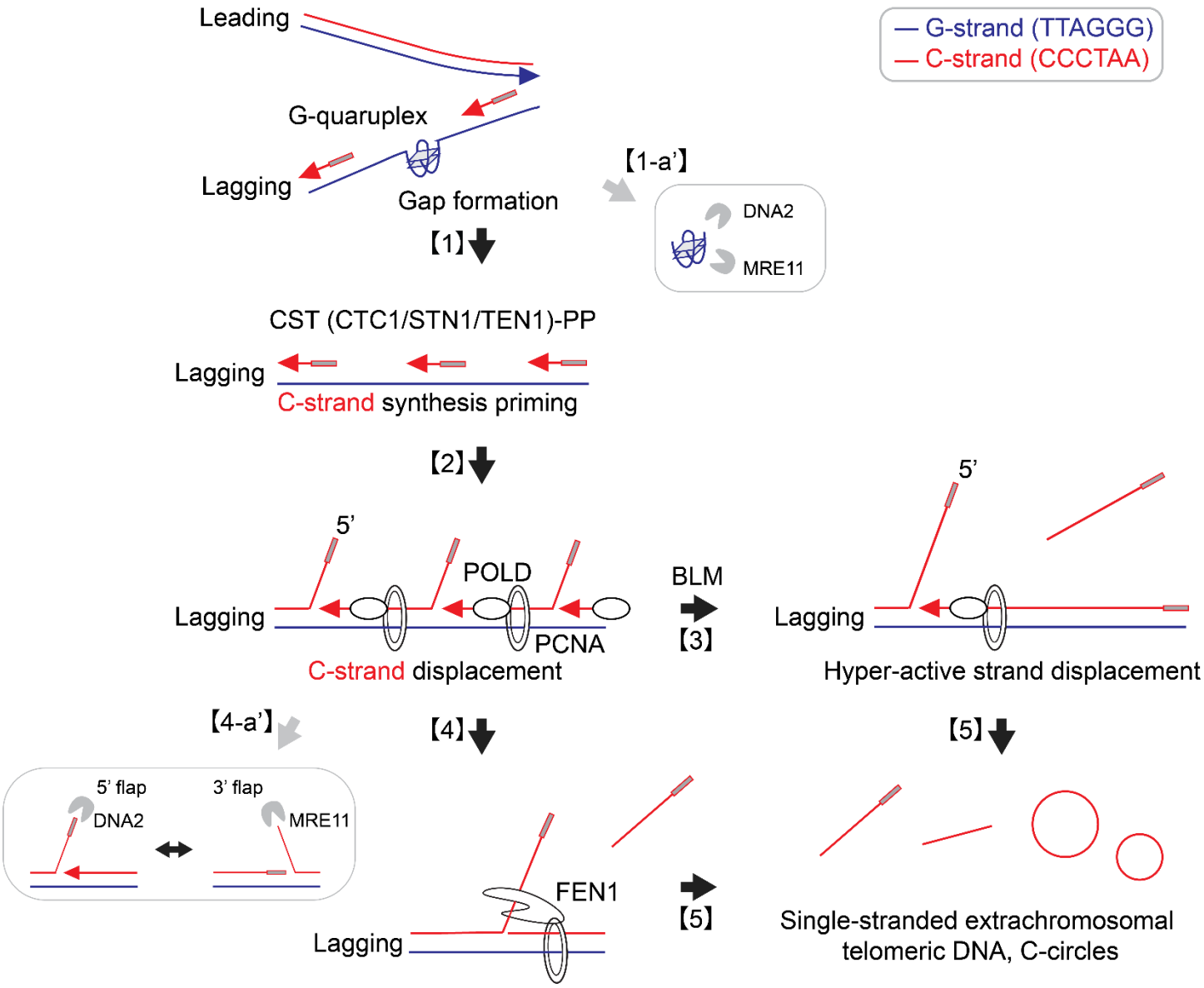

Figure 6. **Origins of C-circles and C-rich single-stranded DNAs: Excessive strand displacements from lagging strand telomeres:** Accumulations of G-quadruplex (G4) structures and G4-associated R-loops at telomeres may contribute to the generation of C-rich single-stranded DNAs (ssDNAs) by potentially exposing parental lagging strands, which can be recognized by the CST-PP (CTC1-STN1-TEN1-Polα-Primase) complex **[1]**. The CST-PP complex exhibits priming activity in the exposed gaps or G4 structures in lagging strands, which are subsequently extended by DNA polymerase delta **[2]**. As a result, primed C-strand Okazaki fragments are initiated by the CST-PP complex and undergo prolonged extension facilitated by DNA polymerase delta and BLM helicase, leading to the formation of long flap structures **[3]**. In the context where long flap structures are not adequately processed by DNA2, the FEN1 nuclease may contribute to the generation of C-rich ssDNAs by cleaving the middle of 5' flap structures **[4]**. Notably, the unique excessive strand displacement activity observed in ALT cells enables the complete displacement of downstream DNA, thereby promoting the accumulation of C-rich single-stranded DNA **[5]**. DNA2 and MRE11 are potentially involved in lagging strand telomere processes by participating in the removal of G4 structures **[1-a']** and processing flap structures in Okazaki fragments on the lagging strands **[4-a']**.